The moderate impact of the 2015 El Niño over East Africa and its representation in seasonal reforecasts

David MacLeod*

Atmospheric, Oceanic and Planetary Physics, University of Oxford, Oxford, UK

Cyril Caminade

Institute of Infection and Global Health, department of Epidemiology and Population Health, University of Liverpool, Liverpool, UK

Corresponding author address: David MacLeod, Atmospheric, Oceanic and Planetary Physics, University of Oxford, Oxford, OX1 3PU, UK

E-mail: macleod@atm.ox.ac.uk

Early Online Release: This preliminary version has been accepted for publication in *Journal of Climate*, may be fully cited, and has been assigned DOI 10.1175/JCLI-D-19-0201.1. The final typeset copyedited article will replace the EOR at the above DOI when it is published.

ABSTRACT

The El Niño Southern Oscillation (ENSO) has large socio-economic impacts worldwide. The positive phase of ENSO, El Niño, has been linked to intense rainfall over Eastern Africa during the short rains season (October-December). However we show here that during the extremely strong 2015 El Niño the precipitation anomaly over most of East Africa during the short rains season was less intense than experienced during previous El Niños, linked to less intense easterlies over the Indian Ocean. This moderate impact was not indicated by reforecasts from the ECMWF operational seasonal forecasting system, SEAS5, which instead forecast large probabilities of an extreme wet signal, with stronger easterly anomalies over the surface of the Indian Ocean and a colder eastern Indian Ocean/western Pacific than was observed. To confirm the relationship of the eastern Indian Ocean to East African rainfall in the forecast for 2015, atmospheric relaxation experiments are carried out which constrain the east Indian Ocean lower troposphere to reanalysis. By doing so the strong wet forecast signal is reduced. These results raise the possibility that link between ENSO and Indian Ocean Dipole events is too strong in the ECMWF dynamical seasonal forecast system and that model predictions for the East African short rains rainfall during strong El Niño events may have a bias toward high probabilities of wet conditions.

Accepted for publication in *Journal of Climate*. DOI 10.1175/JCLI-D-19-0201.1.

1. Introduction

Extreme climate hazards are associated with El Niño events and 2015-2016 saw one of the strongest events ever recorded (Huang et al. (2016)). El Niño is the the warm phase of the El Niño Southern Oscillation (ENSO), and strong events significantly disturb the Walker Cell zonal circulation over the tropics, changing the likelihood of regional drought and flooding across the globe (Vicente-Serrano et al. (2011); Emerton et al. (2017)).

More precisely, the disturbance of circulation patterns induced by El Niño significantly reduces rainfall in Australia, Indonesia and Brazil whilst increasing rainfall over western coastal and southern South America, southern China, eastern Africa and the southern USA during the boreal winter season (Mason and Goddard (2001)). Its impacts are milder during boreal summer, with increased drought conditions observed over India, Australia and Central America (McPhaden et al. (2006)). The largest El Niño events (such as the 1997-98 and 2015-16 events) tend to have the largest impacts on socio-economic factors and the health of population in the tropics, whilst the impacts of weak El Niño events, (such as the 2004-2005 event) are difficult to distinguish from atmospheric background noise (McPhaden et al. (2006)).

The impacts of El Niño on regional rainfall and temperature cascade into significant impacts on agriculture, weather extremes, socio-economic factors and human and animal health (Kovats et al. (2003); McGregor and Ebi (2018); Anyamba et al. (2019)). During El Niño 2015-2016, several catastrophic events took place, such as droughts and disturbance of oceanic temperatures leading to increased bleaching of coral reefs in Australia-Indonesia, droughts depleting livestock numbers and affecting crops in Ethiopia and South Africa and large forest fires affecting Malaysia, Indonesia and neighbouring countries (Claar et al. (2018); International Federation of Red Cross and Red Crescent Societies (2015); Field et al. (2016)). El Niño has also been associated with the

Accepted for publication in *Journal of Climate*. DOI 10.1175/JCLI-D-19-0201.1.

emergence and re-emergence of infectious diseases in the tropics (Hales et al. (1999); Chretien et al. (2015); McGregor and Ebi (2018)).

Large outbreaks of Rift Valley Fever, malaria and cholera over East Africa during the short rains season, increased transmission of dengue and malaria in Latin America and South East Asia during and following the south American and Asian monsoons, and outbreaks of malaria and cholera in India during the Indian monsoon and summer seasons have been reported during large El Niño events (Anyamba et al. (2019)). The recent Zika virus outbreak that plagued Latin America from early 2015 to November 2016 and spread to other countries in Africa and South East Asia was also favoured by regional climate anomalies induced by El Niño (Caminade et al. (2017); Muñoz et al. (2017); Sorensen et al. (2017)).

The strong correlation between the East African short rains (October-December, hereafter OND) and ENSO is well known (Hastenrath et al. (1993); Indeje et al. (2000); Wolff et al. (2011)): significant widespread seasonal rainfall anomalies tend to occur during El Niño events, leading to increased risk of flooding. This was particularly the case during OND 1997 (Nicholson (2017)). A clear fingerprint of strong El Niño events can also be seen on population health in the region: during the 1958-59 El Niño, abnormally high temperature, rainfall and relative humidity resulted in 3 million malaria cases over the highlands of Ethiopia (Fontaine et al. (1961)), whilst during the 1997-98 event, higher temperatures and increased precipitation also resulted in increased malaria prevalence in Kenya (Brown et al. (1998); Omumbo et al. (2011)) and Uganda (Kilian et al. (1999)).

ENSO is understood to influence the short rains over East Africa through the modulation of the Walker-type coupled zonal circulation in the central equatorial Indian Ocean (Mutai and Ward (2000); Hastenrath et al. (2011)). Normal conditions consist of prevailing surface westerlies over the Indian Ocean, easterly flow at 200mb, rising motion in the east and subsidence over the far west

Accepted for publication in *Journal of Climate*. DOI 10.1175/JCLI-D-19-0201.1.

Indian Ocean, supressing rainfall over East Africa. Note that this subsidence cap is at least partly responsible for the unusual occurrence of a semi-arid climate on the equator. Circulation changes induced by El Niño then lead to zonal wind anomalies over the Indian Ocean of an opposite sign to the mean flow, at height (200mb) and near-surface (850mb), corresponding to a weakening of the Walker-type circulation, a reduction of the subsidence cap over East Africa and increased rainfall. In addition to ENSO, the Indian Ocean Dipole (IOD, Saji et al. (1999)) exerts a strong control on the East African short rains (Nicholson (2017)) through the same pathway as ENSO with positive events leading to weakening and potentially reversal of the Walker-type circulation over the Indian Ocean.

During the 2015 short rains, El Niño was at its peak. Seasonal forecast models had well anticipated the onset and strength of the event, with public advisories issued during the first half of 2015 (L'Heureux et al. (2017)). Based on warnings of a strong El Niño event alone, the humanitarian sector conducted preparedness actions for an extreme wet season in East Africa, basing actions on the impacts of similar intensity El Niño events (Tozier de la Poterie et al. (2018)).

However in the event, although some parts of East Africa experienced a particularly wet season, for many other parts (eastern and central Kenya, parts of Somalia) the wet anomaly was not particularly strong; and parts of Ethiopia, Somalia and Tanzania even experienced a drier than average season. Despite the fact that the season coincided with one the largest El Niño event on record, the rainfall impact over East Africa was much less spatially coherent and of lower magnitude compared to impacts during the 1997 event, when the El Niño index was slightly lower than 2015.

The impact of El Niño 2015-16 over the Western US was also unexpected and significant attention has been paid to this event over this region. Here the boreal winter precipitation was much lower than expected from the impact of previous strong El Niño events, and seasonal forecasts

Accepted for publication in *Journal of Climate*. DOI 10.1175/JCLI-D-19-0201.1.

performed poorly for this event (Wanders et al. (2017)). Several studies have examined reasons for this and suggest that internal variability played a significant role (Zhang et al. (2018); Cash and Burls (2019); Lim et al. (2018)), whilst other work found that the weak precipitation in 2015/16 relative to previous major events was likely related to a pattern of tropical SST variability outside of the El Niño core region (Quan et al. (2018)), largely arising from the Indian Ocean and Western Pacific (Siler et al. (2017)).

Little attention has been paid to the details of the impact of the 2015 El Niño over East Africa. However in order to evaluate the reliability of future El Niño-related early warnings it is essential to understand the reasons behind the unexpectedly moderate impact of this particular event in the region, when compared to the impact of historical El Niños. We address this question here through analysis of climate observations and reanalysis. In order to understand the potential of forecasting systems to anticipate 2015 conditions we evaluate dynamical seasonal reforecasts of the season. These reveal high probability forecasts for a particularly wet season to occur, despite the observed dry condition. To diagnose the reasons for this strong signal we describe the results of some atmospheric relaxation experiments. This experimental technique and other methods are described in the following section, which also contains details of the observations and model datasets. Results and discussions follow in sections three and four.

2. Data and methods

a. Observational data

The Climate Hazards group Infrared Precipitation with Stations (CHIRPS Funk et al. (2015)) is used for analysis of precipitation and verification of seasonal reforecasts. CHIRPS is a blend of station and satellite data, providing daily precipitation estimates at 0.05°x0.05° spatial reso-

Accepted for publication in *Journal of Climate*. DOI 10.1175/JCLI-D-19-0201.1.

lution from 1981 to the present. For analysis where precipitation over the ocean is considered, the Global Precipitation Climatology Project (GPCP) data is used (Adler et al. (2003)), which is a monthly precipitation dataset combining satellite and observations on a 2.5° x 2.5° grid. Sea surface temperatures are derived from the HadISST dataset (Rayner (2003)). Dynamic fields to characterise the near-surface circulation (winds, velocity potential and divergent component of winds at 850mb) were derived from the ERA-Interim reanalysis dataset (Dee et al. (2011)). When comparing to model data, all data is interpolated to a 1°x1° grid before analysis.

The Niño 3.4 index is used to characterize ENSO; this index is calculated using the averaged SST anomaly for 5°S-5°N and 170°W-120°W based on HadISST data. The Dipole Mode Index (DMI) is also used in order to characterise the IOD. This is defined as the difference between the average SST in the region 50-70°E and 10°S-10°N minus the average SST in the box 90-110°E and 10°S-0°N. Both the Niño 3.4 and IOD indices were downloaded from the NOAA website (https://www.esrl.noaa.gov/psd/data/climateindices/list/). All analysis has been calculated for OND, corresponding to the the short rains season across most of East Africa.

b. Regression and composite analysis on observational data

In order to explore the relationship between ENSO, the IOD, rainfall, the SSTs and dynamical variables, linear regression coefficients were calculated and compared to anomalies. Anomalies are defined as the departure of each climate variable from its seasonal mean state over 1981-2016. Standardized Niño 3.4 and IOD indices were linearly regressed against detrended climate variables (rainfall, SSTs, velocity potential and divergent component of the wind at 850mb) for OND over the period 1981-2016. The resulting linear regression coefficients, representing the average response of the atmosphere to ENSO and the IOD, were then compared to climate anomalies for the three largest El Niño events occurring during the period considered here: 1982, 1997 and 2015.

Accepted for publication in *Journal of Climate*. DOI 10.1175/JCLI-D-19-0201.1.

Note that composites of climate anomalies on El Niño and La Niña years reveal patterns of similar shape but opposite sign (not shown), indicating that the linearity assumption underlying regression analysis is appropriate.

c. Seasonal forecast data

Seasonal reforecast data from the European Centre for Medium-Range Weather Forecast (ECMWF) and the UK Met Office are analysed in this study, using the forecasts of OND from September start dates across the common reforecast period 1993-2015. Data was retrieved from the Copernicus Data Store (https://climate.copernicus.eu/seasonal-forecasts).

The ECMWF operational seasonal forecast, SEAS5, comprises the integrated forecast system (IFS), an atmospheric model, cycle CY43R1, at Tco319 spatial resolution (about 35km x 35km at the equator), with 91 vertical levels, reaching up to 0.01mb, to an altitude of about 80km. IFS is coupled to the Nucleus for European Modelling of the Ocean (NEMO) ocean model v3.4 on a tripolar 0.25° ORCA grid with 75 vertical levels. Ensemble members are perturbed to account for initial condition and model uncertainty, and 25 ensemble members are available for the reforecast.

The UK Met Office seasonal forecasting system is GloSea5, which is a coupled model based on the MetUM atmospheric model, the JULES land surface model, the NEMO ocean model and the Los-Alamos sea-ice model (MacLachlan et al. (2015)). The atmospheric model has spatial resolution of 0.83° (longitude) by 0.56° (latitude), with 85 levels in the atmosphere and a top at 85km. The spatial resolution of NEMO is 0.25° on a tri-polar ORCA grid, with 75 vertical levels. 28 perturbed ensemble members are available in the reforecast.

Accepted for publication in *Journal of Climate*. DOI 10.1175/JCLI-D-19-0201.1.

d. Atmospheric relaxation experiments

Analysis of SEAS5 forecast reveals high forecast probabilities for a very wet season over East Africa (see results section). In order to explore the mechanisms responsible for such a wet signal, relaxation experiments are carried out. These follow the technique described in (Jung (2011)), where the atmosphere is nudged back toward observations (in this case ERA-Interim reanalysis) at every timestep, inside a specified region. Outside of the region the coupled modeling system is allowed to evolve freely. Note that the current study differs from Jung (2011) in that the method is applied to a coupled atmosphere-ocean model, rather than an atmosphere-only model.

The control simulation is a 25 member, four month reforecast initialised on the 1st of September, using the ECMWF-IFS atmosphere model coupled to the NEMO ocean model and initialised with ERA-Interim atmospheric reanalyses and ORAS4 oceanic reanalysis. The resolution of the atmospheric model for the relaxation experiments is T255, cycle CY41R1 (N.B. this differs from SEAS5 resolution and cycle, which is currently too computationally expensive to use in research mode; however the forecast for 2015 in the experimental control is similar to that seen in the SEAS5 reforecast).

A series of 25 members relaxation experiments were then performed. These follow the control setup, but where remote regions are relaxed towards ERA-Interim. Regions in the eastern Indian Ocean were chosen based on differences between the 2015 and 1997 event seen in analysis of reanalysis and reforecasts, presented later. The regions are shown in figure 1. The first corresponds to the eastern box used to defined the IOD index, that is 90-110°E, 0-10°S (experiment IOD2 hereafter). Extending westward from this box, the second region used was 70-110°E, 0-10°S (IOD2+). Finally, a third region extended northward of the equator, covering 70-110°E 10°N-10°S (experiment IOD2++). In each case, zonal and meridional wind, humidity and temperature

Accepted for publication in *Journal of Climate*. DOI 10.1175/JCLI-D-19-0201.1.

at atmospheric levels below 700mb were relaxed back toward ERA-Interim on a 6-hour timestep, with logarithmic spatial smoothing at the domain boundaries in order to avoid discontinuities.

3. Results

a. Impacts of the 2015 El Niño on East Africa short rains

Figure 2 shows rainfall during the three highest El Niño years since 1981 according to CHIRPS precipitation data over East Africa, showing the ranking of the year at each point (figure 2a-c) as well as standardized rainfall anomalies (figures 2d-f). During the 1997 event, the region experienced one of the largest precipitation anomalies on record, with significant parts of Kenya, Somalia and Ethiopia showing wet anomalies three standard deviations above the mean (figure 2e). 1982 saw a weaker El Niño, though most of the region experienced rainfall anomalies one standard deviation above the mean, and parts of southern Kenya saw the wettest season on record (figure 2d). During 2015, rainfall was much lower than seen in previous El Niños (figure 2f); over the Mandera triangle region where Kenya, Somalia and Ethiopia meet, the anomalies were close to the climatological mean. Uganda experienced the wettest season on record, central Somalia saw a high precipitation anomaly while drier than average conditions were observed over Somalia, Ethiopia and Tanzania.

Rainfall anomalies in 2015 were much lower and less spatially coherent than in 1997. Given that the IOD has been shown to be a key driver of the East African short rains (Black et al. (2003); Black (2005)), it is possible that this phenomena played a role in the difference between 2015 and 1997 impacts. Indeed, the strongest IOD on record occurred in 1997, with an index over twice the magnitude as observed in 1982 and 2015 (figure 2a-c, inset). In order to evaluate the relative

Accepted for publication in *Journal of Climate*. DOI 10.1175/JCLI-D-19-0201.1.

influence of ENSO and IOD on East African climate, we compare the average impact of ENSO and IOD on dynamic variables and precipitation in the Tropics.

The average impact of ENSO and the IOD is estimated using linear regression and compared to the observed anomalies for 1982, 1997 and 2015; results are shown in figure 3. Positive phases of both ENSO and the IOD are associated with increased low level 850mb easterly zonal wind anomalies over the Indian Ocean (figure 3f, g), increased surface divergence and drought conditions over Indonesia-Malaysia and Brazil, increased convergence and consequently increased rainfall conditions over East Africa (figure 3a, b). However the strength of this relationship with the IOD is much stronger than with ENSO, with much stronger easterly wind anomalies, reaching further into the west of the Indian Ocean and the eastern coasts of Africa. Consistently, the average response to the IOD index indicates larger positive rainfall anomalies over East Africa (figure 3b) compared to ENSO (figure 3a). This indicates that whilst both ENSO and IOD are associated with a reversal of the Indian Ocean walker cell, the impacts of the IOD on East African climate tend to be larger. This finding is consistent with previous work (Nicholson (2017)). For reference, the regression of climate fields onto an East Africa OND precipitation index (supplementary figure 1) confirms the strong association between OND rainfall and the zonal wind pattern associated with the IOD.

The 1997 event projects both on positive phases of ENSO and IOD (figure 3d, i, n) and is consistently associated with much stronger easterly wind anomalies over the Indian ocean (figure 3i), and consequently larger rainfall anomalies over the western part of the Indian Ocean and Eastern Africa (figure 3d). Regional climate anomalies related to the 1982 (figure 3c, h, m) and 2015 events (figure 3e, j, o) tend to be in closer agreement with regression patterns calculated using the Niño 3.4 index (figure 3a, e, j), with weaker easterly wind anomalies over the Indian ocean and more moderate rainfall anomalies reaching the coasts of Eastern Africa. These results

Accepted for publication in *Journal of Climate*. DOI 10.1175/JCLI-D-19-0201.1.

suggest that the moderate impact of the 2015 El Niño on East African rainfall compared to 1997 is linked to weaker IOD-like activity in the Indian Ocean, with no strong cold SST in the east and weaker 850mb easterly wind anomalies crossing the Indian basin. With this understanding of the differences between the 2015 event and the canonical El Niño response, we turn to the representation of this event in operational seasonal forecasts.

b. Seasonal forecasts of the 2015 short rains

The consensus seasonal outlook from the Greater Horn of Africa Regional Outlook Forum (GHACOF) is shown in figure 4. This forecast was issued at the 41st GHACOF meeting held in August 2015 in Dar Es Salaam, Tanzania, just two months before the start of the short rains. At that time the evolution towards a strong El Niño was clearly indicated across all dynamical models (L'Heureux et al. (2017)). The consensus rainfall outlook indicated that a probability of 45% was given for upper tercile rainfall over a large region covering most of Kenya and the Mandera triangle which ultimately did not experience such significant flooding. Note that a probability of 45% is at the top of the range of increased probabilities issued at the GHACOF meeting, which tend to be conservative, see Mason and Simbarashe (2009) for further assessment of the issued probabilities and reliability of Regional Climate Outlook Forum. This outlook is based on a consensus of multiple information streams: forecasts issued by national East African meteorological centres, in-house statistical models, the analogue year approach, as well as dynamical forecasts issued by the WMO-designated Global Producing Centres (GPCs, see https://www.wmolc.org/ for further details).

The evolution of a strong El Niño in 2015 was anticipated months in advance, in both the ECMWF and the UK Met Office operational seasonal forecast systems SEAS5 and GloSea5 (Ineson et al. (2018)). Figure 5 shows precipitation anomaly forecast for East Africa for these two

Accepted for publication in *Journal of Climate*. DOI 10.1175/JCLI-D-19-0201.1.

forecasting systems at a one month lead time for OND (forecast initialized in September). Both systems indicated overall wet conditions over East Africa (figure 5e-g, i-k). However the SEAS5 ensemble overwhelmingly forecast a large wet event, raising the probability of an upper quintile event (80th percentile, 1 in 5 year) to over 50% across the region, and over 70% in some places (figure 5g). However as shown by CHIRPS observations (figure 5c), the region actually experiencing an upper quintile rainfall event was restricted to Uganda, southern Kenya, and a small part of Somalia and Ethiopia. SEAS5 did not capture the spatial variability in the event and instead indicated strong wet anomalies across the entire East African region, in a similar way to the pattern observed in 1997. GloSea5 also indicated increased probabilities of such a wet event to occur, with a higher probability of an upper quintile event to occur over Uganda, southern Somalia, western Kenya and most of Tanzania and normal probabilities shown in the Mandera triangle region, however the spatial pattern of GloSea5 anomalies are more consistent with observations, whilst the probabilities of an upper quintile event were lower than SEAS5.

Observed and predicted sea surface temperature (SST) anomalies are also shown in figure 5c, f & i. HadISST observed anomalies depict the strong El Niño event in the Pacific and warming across the Indian Ocean. Warm anomalies are observed in the western Indian Ocean, with normal conditions in the eastern part, corresponding to a positive IOD event. Ensemble mean anomalies from the two forecast systems indicate a realistic representation of the spatial pattern of warming in the Pacific, including the warm blob off the coasts of California (Tseng et al. (2017)). However though both systems captured the warming in the west Indian Ocean, the SEAS5 ensemble overestimates the zonal SST gradient across the basin and simulated -1K cold anomalies in the east Indian Ocean with generally cold conditions across the Maritime Continent. By contrast, the GloSea5 ensemble mean SST anomalies in the east were more closely aligned with observations.

Accepted for publication in *Journal of Climate*. DOI 10.1175/JCLI-D-19-0201.1.

These results are consistent with (Black et al. (2003)), who demonstrated that extreme rainfall over East Africa only occurs when the zonal SST gradient over the Indian Ocean reverses for several months. In order to look in more detail within the SEAS5 ensemble, anomalies predicted by individual ensemble members are shown in supplementary figures 2-5. For precipitation nearly all members indicate wet anomalies, although it should be noted that at least one ensemble members is as dry as the observations, so the actual outcome did fall within the range of the forecast ensemble (supplementary figure 2). Circulation patterns are shown as departures from the ensemble mean in supplementary figure 3-4 for 850mb and 200mb zonal wind. There is no clear systematic relationship within the ensemble between circulation and precipitation: there is a slight tendency for wetter members to have easterly (negative zonal wind) 850mb anomalies near the Kenya coast, consistent with the interannual relationship with the Indian Ocean Walker circulation, however this is not apparent for all members. For instance, the very wettest member also has the most westerly winds in the West Indian Ocean.

However analysis of the SST anomalies predicted by the ensemble (supplementary figure 5) reveals that all members have a similar distinct 'cold tongue' in Indian Ocean, consisting of relatively sharp meridional gradients. This cold tongue stretches out from Indonesia into the central Indian Ocean and is visible in the ensemble mean, but is not present in the observed SST (figure 5); all SEAS5 ensemble members predict sharper meridional gradients than observed. This suggests a systematic error in the East Indian Ocean and tendency to overestimate the chance of a positive IOD in the Indian Ocean given an El Niño in the Pacific, along with errors in the spatial structure of SST anomalies in the East Indian Ocean. It is hypothesised that this bias was largely responsible for the large positive precipitation anomaly forecast over East Africa. Seasonal forecast relaxation experiments have then been carried out to test this hypothesis and results are described in the next section.

Accepted for publication in *Journal of Climate*. DOI 10.1175/JCLI-D-19-0201.1.

c. Relaxation experiments to investigate the source of the strong wet signal in SEAS5

The impact of the relaxation experiments on simulated OND 2015 conditions relative to the control experiment is shown in figure 6 (for reference the mean and anomalies for each experiment are shown in supplementary figures 6 & 7). All three experiments which relax the atmosphere towards reanalyses over the eastern Indian Ocean lead to a reduction in the simulated cold SST anomaly there compared to the control (figure 6j-l). However the magnitude of the impact on dynamics outside of this region depends on the extent of the relaxation box used.

In the IOD2 experiment some impact is seen on the zonal wind fields (figure 6a, d). Equatorial 850mb easterly anomalies are reduced in the central Indian Ocean, whilst the 200mb easterly anomalies south of the equator are reduced. This leads to a drier precipitation signal in the western Indian Ocean and a wetter signal in the east (figure 6g); consistent with a smaller westward extension of the surface zonal wind anomalies and a more eastward location of convergent winds. However no significant impact is seen on the continental precipitation signal over East Africa.

By extending the relaxation box to the central Indian Ocean (experiment IOD2+), a larger impact on the precipitation signal over the Indian Ocean is shown (figure 6h), whilst the impact on 850mb zonal winds is slightly higher and the impact on the 200mb winds extends to a larger region (figures 6b, e). However no significant difference in the precipitation signal over East Africa is seen in the IOD2+ experiment either (figure 6h).

Only the IOD2++ experiment shows widespread significant drying of the precipitation signal over East Africa with respect to the control (figure 6i). This is accompanied by a larger impact on the 200mb wind anomalies compared to the IOD2 and IOD2+ experiments and a slightly larger extent of impact on the 850mb zonal wind fields (figures 6c, f). Outside of East Africa, the impact of this experiment on precipitation leads to a strong drying signal all across the western Indian

Accepted for publication in *Journal of Climate*. DOI 10.1175/JCLI-D-19-0201.1.

Ocean, extending into the east, with significant wetting north and south of the dry signal. The IOD2++ experiment also leads to a cooling of the equatorial Pacific in the Niño region, demonstrating that the link between ENSO and the Indian Ocean is not a one-way forcing; the Indian Ocean has the potential to moderate El Niño events.

The rainfall reduction over the East Africa is only apparent for the IOD2++ experiment which extends the relaxation box across the eastern Indian Ocean. This suggests that model errors are not confined to the traditional spatial domain used to define the eastern pole of the IOD, rather that coupled near-surface processes in the Indian Ocean west of 70°E and both sides of the equator are important. This reduction is in the wet signal over the Indian Ocean across the experiments is proportional to the size of the impact on both 850mb and 200mb winds, with larger reductions coincident with a reduction in the size of near-surface easterly anomalies and an increase in the size of westerly anomalies at height, consistent with a weaker reduction in the strength of the Walker-type circulation in the relaxation experiments.

Specifically, a tendency toward too-cold SST anomalies in SEAS5 for 2015 led to a reduction in convection over the Maritime Continent, leading to both reduced convergence at the surface and divergence aloft. These simultaneously led to a reduction in the strength of the Walker-type circulation over the Indian Ocean, thereby increasing the wet signal over East Africa through reduced moisture flux away from the continent at the surface and enhanced potential for deep convection through reduced convergence aloft. The accompaniment of the strong reduction in the East Africa dry signal in the IOD2++ experiment by a particularly strong increase in the impact on the 200mb zonal wind points in particular to the upper branch of the Indian Ocean walker cell as a key player in modulating the impacts of the 2015 El Niño on East African rainfall.

Accepted for publication in *Journal of Climate*. DOI 10.1175/JCLI-D-19-0201.1.

4. Discussion and conclusions

2015 experienced one of the strongest El Niño on record and the humanitarian preparedness response was based largely on impacts observed during previous large El Niño events. However though some parts of East Africa experienced a particularly wet season, for most regions the wet anomaly was not particularly large and some parts even experienced a drier than average season. This was due to a positive but weaker IOD phase compared to previous El Niño events (such as as the 1997 event) and led to a smaller reduction in the strength of the Indian Ocean Walker-type circulation.

Seasonal forecasts well anticipated the strong El Niño event of 2015, however at one month lead the operational ECMWF SEAS5 reforecast indicates large probabilities of an extreme wet season which didn't happen in many regions, along with a too-strong zonal SST gradient in the Indo-Pacific basin. In addition systematic errors were found in the structure of SST anomalies in the East Indian Ocean in the reforecast ensemble, where sharp meridional gradients of SST were present in every ensemble member but not seen in observations.

Relaxation experiments confirm that the eastern Indian Ocean atmosphere-ocean below 700mb is the source of the high forecast probabilities of wet conditions. By nudging the atmosphere in this region toward observations the model simulates a weaker reversal of the Walker cell and reproduces a more realistic drier signal over East Africa in 2015. Interestingly the experiment which leads to drying over East Africa also shows widespread significant impacts on the 200mb zonal wind fields, suggesting that the upper branch of the cell and associated impacts on upper tropospheric divergence were a key factor in the 2015 event over East Africa. Further work to explore this link might consider additional relaxation experiments where a region is relaxed to an alternative year. For example, a reforecast of 1997 could relax the East Indian Ocean to 2015, to

Accepted for publication in *Journal of Climate*. DOI 10.1175/JCLI-D-19-0201.1.

see to what extent activity here would modify the wet signal over East Africa. Another alternative would be atmosphere-only forced-SST initialized seasonal reforecasts to test the sensitivity of East African rainfall to the magnitude and position of SST anomalies in the East Indian ocean.

Work to understand the unexpectedly moderate response of the 2015-16 El Niño over the US has suggested that response was related to internal atmospheric variability. In particular Zhang et al. (2018) suggest a particularly active Madden-Julian Oscillation (MJO) during the season was an important factor. However MJO activity is unable to explain the moderate response over East Africa, where an active MJO in phase 2-4 is normally associated with particularly wet periods (Berhane and Zaitchik (2014); Zaitchik (2017)). MJO activity over OND 1997 and 2015 (supplementary figure 8) shows an inactive MJO in 1997 whilst 2015 had MJO particularly in phase 2-4 in 2015. Given this alone one would expect 2015 to be wetter than 1997.

However despite clear differences between East African and Western US climate, results may be compared the work of Siler et al. (2017), who link the dry conditions over the Western US to a dipole pattern of SST variability across the Indian Ocean and West Pacific; a pattern resembling the IOD. This pattern of SST variability was not well captured by seasonal forecasts from the North American Multimodel Ensemble, which had erroneous predictions of above-average precipitation in the West US. The Indian Ocean response to the 2015 El Niño and the inability of most seasonal forecast models to capture the SST pattern corresponding to a mild IOD may have then impacted East Africa in addition to the Western US.

The impact of strong IOD events on East Africa climate has been demonstrated previously: IOD events which reverse zonal SST gradient over the Indian basin for several months trigger extreme rainfall over the region (Black et al. (2003)). Though IOD events are often triggered by Pacific ENSO they can also occur independently (Schott et al. (2009)). However a study of preparedness responses during 2015 indicated that humanitarian actors solely based actions on the impacts of

Accepted for publication in *Journal of Climate*. DOI 10.1175/JCLI-D-19-0201.1.

similar intensity El Niño and did not consider the state of the Indian Ocean at all (Tozier de la Poterie et al. (2018)).

The implication of these results for the humanitarian sector working in East Africa is that they should not rely on ENSO outlooks in isolation to guide preparedness actions, and should not assume that the impacts of the next El Niño will be similar to former events. The state of the Indian Ocean is also critical in modulating East African short rains, the IOD in particular. The output of coupled climate model forecasts has the potential to provide more accurate warnings than an 'analogue year' approach to early intervention, however a close examination of predictability and model skill is necessary if forecasts are to be relied upon (Kilavi et al. (2018)).

It is important to note that the SEAS5 increased probabilities of an extreme wet season were not necessarily 'wrong': strictly, it is impossible to say if a single probabilistic forecast is wrong or right (as long as 0 or 100% probabilities are not issued). In 2015, over most of the region the SEAS5 probability that the rainfall would be above the upper quintile was around 50%: this corresponds to a probability of around 50% that the rainfall will *not* be above the upper quintile. Indeed, looking at all 25 individual SEAS5 ensemble members over East Africa shows at least one member as dry as the observations (supplementary figure 2). That is, although the SEAS5 ensemble overall had a strong wet signal, the verification observations still fall within the range of possible futures estimated by the model. In addition, it should be made clear that this research considers a particular 'edge case', rather than overall seasonal forecast performance. This has been assessed across the whole SEAS5 hindcast, demonstrating that in general SEAS5 performs particularly well the East African short rains (see MacLeod (2019a,b) for further details).

However the results here lead to the hypothesis that SEAS5 has a systematic bias toward strong positive IOD events during strong El Niños. This is consistent with previous work showing a significant over-estimation of the correlation between Indian Ocean and Pacific rainfall anomalies

Accepted for publication in *Journal of Climate*. DOI 10.1175/JCLI-D-19-0201.1.

(Molteni et al. (2015)). With only a small sample of strong El Niño events in the seasonal reforecast period it is difficult make a robust claim of this link. However future work will look at 110-year experimental reforecast of the ECMWF seasonal prediction system (a coupled version of that system is described in Weisheimer et al. (2017)) which may shed further light on this question This will help to better understand the behaviour of start-of-the-art coupled climate models in order to improve rainfall predictions over East Africa.

Acknowledgments. DM is supported by the NERC/DfID project ForPAc: Toward Forecast-based Preparedness Action (NE/P000673/1). CC was funded by the NERC project 'Impact of El Niño on malaria vector dynamics in Tanzania: observation, improvement and unleashing forecasting potential' (NE/P004407/1) as well as by the National Institute for Health Research Health Protection Research Unit in Emerging and Zoonotic Infections at the University of Liverpool in partnership with Public Health England and Liverpool School of Tropical Medicine. The views expressed are those of the authors and not necessarily those of the NHS, the NIHR, the Department of Health or Public Health England. Reforecast and reanalysis data was downloaded from the Copernicus Data Store, CHIRPS data from the Climate Hazards Group of UCSB and climate model experiments were carried out using a member state special project at ECMWF, where data is archived (details available on request).

References

Adler, R. F., and Coauthors, 2003: The Version-2 Global Precipitation Climatology Project (GPCP) Monthly Precipitation Analysis (1979 - Present). *Journal of Hydrometeorology*, **4 (6)**, 1147–1167, doi:10.1175/1525-7541(2003)004⟨1147:TVGPCP⟩2.0.CO;2.

Accepted for publication in *Journal of Climate*. DOI 10.1175/JCLI-D-19-0201.1.

Anyamba, A., and Coauthors, 2019: Global disease outbreaks associated with the 2015–2016 el niño event. *Scientific reports*, **9 (1)**, 1930.

Berhane, F., and B. Zaitchik, 2014: Modulation of Daily Precipitation over East Africa by the Madden–Julian Oscillation*. *Journal of Climate*, **27 (15)**, 6016–6034, doi:10.1175/JCLI-D-13-00693.1, URL http://journals.ametsoc.org/doi/abs/10.1175/MWR3026.1.

Black, E., 2005: The relationship between Indian Ocean sea-surface temperature and East African rainfall. *Philosophical transactions. Series A, Mathematical, physical, and engineering sciences*, **363 (1826)**, 43–47, doi:10.1098/rsta.2004.1474.

Black, E., J. Slingo, and K. R. Sperber, 2003: An Observational Study of the Relationship between Excessively Strong Short Rains in Coastal East Africa and Indian Ocean SST. *Monthly Weather Review*, **131 (1)**, 74–94, doi:10.1175/1520-0493(2003)131⟨0074:AOSOTR⟩2.0.CO;2, URL http://journals.ametsoc.org/doi/abs/10.1175/1520-0493%282003%29131%3C0074%3AAOSOTR%3E2.0.CO%3B2.

Brown, V., M. Abdir Issak, M. Rossi, P. Barboza, and A. Paugam, 1998: Epidemic of malaria in north-eastern Kenya. *Lancet (London, England)*, **352 (9137)**, 1356–7, doi:10.1016/S0140-6736(05)60747-7, URL http://www.ncbi.nlm.nih.gov/pubmed/9802279.

Caminade, C., J. Turner, S. Metelmann, J. C. Hesson, M. S. C. Blagrove, T. Solomon, A. P. Morse, and M. Baylis, 2017: Global risk model for vector-borne transmission of Zika virus reveals the role of El Niño 2015. *Proceedings of the National Academy of Sciences*, **114 (1)**, 119–124, doi:10.1073/pnas.1614303114, URL http://www.ncbi.nlm.nih.gov/pubmed/27994145http://www.pubmedcentral.nih.gov/articlerender.fcgi?artid=PMC5224381http://www.pnas.org/lookup/doi/10.1073/pnas.1614303114.

Accepted for publication in *Journal of Climate*. DOI 10.1175/JCLI-D-19-0201.1.

Cash, B. A., and N. J. Burls, 2019: Predictable and unpredictable aspects of us west coast rainfall and el niño: Understanding the 2015/16 event. *Journal of Climate*, **32 (10)**, 2843–2868.

Chretien, J.-P., A. Anyamba, J. Small, S. Britch, J. L. Sanchez, A. C. Halbach, C. Tucker, and K. J. Linthicum, 2015: Global Climate Anomalies and Potential Infectious Disease Risks: 2014-2015. *PLoS Currents*, doi:10.1371/currents.outbreaks.95fbc4a8fb4695e049baabfc2fc8289f, URL http://currents.plos.org/outbreaks/?p=50798.

Claar, D. C., L. Szostek, J. M. McDevitt-Irwin, J. J. Schanze, and J. K. Baum, 2018: Global patterns and impacts of el niño events on coral reefs: A meta-analysis. *PloS one*, **13 (2)**, e0190 957.

Dee, D. P., and Coauthors, 2011: The ERA-Interim reanalysis: configuration and performance of the data assimilation system. *Quarterly Journal of the Royal Meteorological Society*, **137 (656)**, 553–597, doi:10.1002/qj.828, URL http://doi.wiley.com/10.1002/qj.828.

Emerton, R., H. L. Cloke, E. M. Stephens, E. Zsoter, S. J. Woolnough, and F. Pappenberger, 2017: Complex picture for likelihood of ENSO-driven flood hazard. *Nature Communications*, **8**, doi:10.1038/ncomms14796.

Field, R. D., and Coauthors, 2016: Indonesian fire activity and smoke pollution in 2015 show persistent nonlinear sensitivity to el niño-induced drought. *Proceedings of the National Academy of Sciences*, **113 (33)**, 9204–9209.

Fontaine, R. E., A. E. Najjar, and J. S. Prince, 1961: The 1958 Malaria Epidemic in Ethiopia. *The American Journal of Tropical Medicine and Hygiene*, **10 (6)**, 795–803, doi:10.4269/ajtmh.1961.10.795, URL http://www.ajtmh.org/content/journals/10.4269/ajtmh.1961.10.795.

Accepted for publication in *Journal of Climate*. DOI 10.1175/JCLI-D-19-0201.1.

Funk, C., and Coauthors, 2015: The climate hazards infrared precipitation with stations—a new environmental record for monitoring extremes. *Scientific Data*, **2**, 150 066, doi:10.1038/sdata.2015.66, URL http://www.nature.com/articles/sdata201566.

Hales, S., P. Weinstein, Y. Souares, and A. Woodward, 1999: El Niño and the dynamics of vector-borne disease transmission. *Environmental health perspectives*, **107 (2)**, 99–102, doi:10.1289/ehp.9910799, URL http://www.ncbi.nlm.nih.gov/pubmed/9924003http://www.pubmedcentral.nih.gov/articlerender.fcgi?artid=PMC1566321.

Hastenrath, S., A. Nicklis, and L. Greischar, 1993: Atmospheric-hydrospheric mechanisms of climate anomalies in the western equatorial Indian Ocean. *Journal of Geophysical Research*, **98 (C11)**, 20 219, doi:10.1029/93JC02330, URL http://doi.wiley.com/10.1029/93JC02330.

Hastenrath, S., D. Polzin, and C. Mutai, 2011: Circulation mechanisms of kenya rainfall anomalies. *Journal of Climate*, **24 (2)**, 404–412, doi:10.1175/2010JCLI3599.1.

Huang, B., M. L'Heureux, Z.-Z. Hu, and H.-M. Zhang, 2016: Ranking the strongest ENSO events while incorporating SST uncertainty. *Geophysical Research Letters*, **43 (17)**, 9165–9172, doi:10.1002/2016GL070888, URL http://doi.wiley.com/10.1002/2016GL070888.

ICPAC, 2015: Statement from the 41st Greater Horn of Africa Climate Outlook Forum, Kunduchi Beach Hotel, Dar es Salaam, Tanzania. Tech. rep. URL https://perma.cc/9C2X-PHRU.

Indeje, M., F. H. Semazzi, and L. J. Ogallo, 2000: Enso signals in east african rainfall seasons. *International journal of Climatology*, **20 (1)**, 19–46.

Ineson, S., and Coauthors, 2018: Predicting El Niño in 2014 and 2015. *Scientific Reports*, **8 (1)**, doi:10.1038/s41598-018-29130-1.

Accepted for publication in *Journal of Climate*. DOI 10.1175/JCLI-D-19-0201.1.

International Federation of Red Cross and Red Crescent Societies, 2015: Emergency Plan of Action update. Ethiopia: Drought. URL http://adore.ifrc.org/Download.aspx?FileId=156069.

Jung, T., 2011: Diagnosing remote origins of forecast error: Relaxation versus 4D-Var data-assimilation experiments. *Quarterly Journal of the Royal Meteorological Society*, **137 (656)**, 598–606, doi:10.1002/qj.781.

Kilavi, M., and Coauthors, 2018: Extreme Rainfall and Flooding over Central Kenya Including Nairobi City during the Long-Rains Season 2018: Causes, Predictability, and Potential for Early Warning and Actions. *Atmosphere*, **9 (12)**, 472, doi:10.3390/atmos9120472, URL http://www.mdpi.com/2073-4433/9/12/472.

Kilian, A., P. Langi, A. Talisuna, and G. Kabagambe, 1999: Rainfall pattern. El Niño and malaria in Uganda. *Transactions of the Royal Society of Tropical Medicine and Hygiene*, **93 (1)**, 22–23, doi:10.1016/S0035-9203(99)90165-7, URL https://academic.oup.com/trstmh/article-lookup/doi/10.1016/S0035-9203(99)90165-7.

Kovats, R. S., M. J. Bouma, S. Hajat, E. Worrall, and A. Haines, 2003: El Niño and health. *The Lancet*, **362 (9394)**, 1481–1489, doi:10.1016/S0140-6736(03)14695-8, URL http://www.ncbi.nlm.nih.gov/pubmed/14602445https://linkinghub.elsevier.com/retrieve/pii/S0140673603146958.

Lim, Y.-K., S. D. Schubert, Y. Chang, A. M. Molod, and S. Pawson, 2018: The impact of sst-forced and unforced teleconnections on 2015/16 el niño winter precipitation over the western united states. *Journal of Climate*, **31 (15)**, 5825–5844, doi:10.1175/JCLI-D-17-0218.1, URL https://doi.org/10.1175/JCLI-D-17-0218.1.

Accepted for publication in *Journal of Climate*. DOI 10.1175/JCLI-D-19-0201.1.

L'Heureux, M. L., and Coauthors, 2017: Observing and Predicting the 2015/16 El Niño. *Bulletin of the American Meteorological Society*, **98 (7)**, 1363–1382, doi:10.1175/BAMS-D-16-0009.1, URL http://journals.ametsoc.org/doi/10.1175/BAMS-D-16-0009.1.

MacLachlan, C., and Coauthors, 2015: Global Seasonal forecast system version 5 (GloSea5): a high-resolution seasonal forecast system. *Quarterly Journal of the Royal Meteorological Society*, **141 (689)**, 1072–1084, doi:10.1002/qj.2396, URL http://doi.wiley.com/10.1002/qj.2396.

MacLeod, D., 2019a: Seasonal forecast skill over the Greater Horn of Africa: a verification atlas of System 4 and SEAS5. Part 1: Precipitation. Tech. rep. URL https://www.ecmwf.int/node/18906.

MacLeod, D., 2019b: Seasonal forecast skill over the Greater Horn of Africa: a verification atlas of System 4 and SEAS5. Part 2: 2m Temperature. Tech. rep. URL https://www.ecmwf.int/node/18923.

Mason, S., and C. Simbarashe, 2009: IRI Position paper: Verification of African RCOF forecasts. Tech. rep. doi:10.7916/D85T3SB0.

Mason, S. J., and L. Goddard, 2001: Probabilistic precipitation anomalies associated with enso. *Bulletin of the American Meteorological Society*, **82 (4)**, 619–638.

McGregor, G., and K. Ebi, 2018: El Niño Southern Oscillation (ENSO) and Health: An Overview for Climate and Health Researchers. *Atmosphere*, **9 (7)**, 282, doi:10.3390/atmos9070282, URL http://www.mdpi.com/2073-4433/9/7/282.

McPhaden, M. J., S. E. Zebiak, and M. H. Glantz, 2006: ENSO as an integrating concept in earth science. *Science (New York, N.Y.)*, **314 (5806)**, 1740–5, doi:10.1126/science.1132588, URL http://www.ncbi.nlm.nih.gov/pubmed/17170296.

Accepted for publication in *Journal of Climate*. DOI 10.1175/JCLI-D-19-0201.1.

Molteni, F., T. N. Stockdale, and F. Vitart, 2015: Understanding and modelling extra-tropical teleconnections with the Indo-Pacific region during the northern winter. *Climate Dynamics*, **45 (11-12)**, 3119–3140, doi:10.1007/s00382-015-2528-y, URL http://link.springer.com/10.1007/s00382-015-2528-y.

Muñoz, Á. G., M. C. Thomson, A. M. Stewart-Ibarra, G. A. Vecchi, X. Chourio, P. Nájera, Z. Moran, and X. Yang, 2017: Could the Recent Zika Epidemic Have Been Predicted? *Frontiers in Microbiology*, **8**, 1291, doi:10.3389/fmicb.2017.01291, URL http://www.ncbi.nlm.nih.gov/pubmed/28747901http://www.pubmedcentral.nih.gov/articlerender.fcgi?artid=PMC5506221http://journal.frontiersin.org/article/10.3389/fmicb.2017.01291/full.

Mutai, C. C., and M. N. Ward, 2000: East African rainfall and the tropical circulation/convection on intraseasonal to interannual timescales. *Journal of Climate*, doi:10.1175/1520-0442(2000)013⟨3915:EARATT⟩2.0.CO;2.

Nicholson, S. E., 2017: Climate and climatic variability of rainfall over eastern Africa. *Reviews of Geophysics*, **55 (3)**, 590–635, doi:10.1002/2016RG000544.

Omumbo, J. A., B. Lyon, S. M. Waweru, S. J. Connor, and M. C. Thomson, 2011: Raised temperatures over the Kericho tea estates: revisiting the climate in the East African highlands malaria debate. *Malaria Journal*, **10 (1)**, 12, doi:10.1186/1475-2875-10-12, URL http://malariajournal.biomedcentral.com/articles/10.1186/1475-2875-10-12.

Quan, X.-W., M. Hoerling, L. Smith, J. Perlwitz, T. Zhang, A. Hoell, K. Wolter, and J. Eischeid, 2018: Extreme california rains during winter 2015/16: A change in el niño teleconnection? *Bulletin of the American Meteorological Society*, **99 (1)**, S49–S53.

Accepted for publication in *Journal of Climate*. DOI 10.1175/JCLI-D-19-0201.1.

Rayner, N. A., 2003: Global analyses of sea surface temperature, sea ice, and night marine air temperature since the late nineteenth century. *Journal of Geophysical Research*, **108 (D14)**, 4407, doi:10.1029/2002JD002670, URL http://dx.doi.org/10.1029/2002JD002670http://www.agu.org/pubs/crossref/2003/2002JD002670.shtml.

Saji, N. H., B. N. Goswami, P. N. Vinayachandran, and T. Yamagata, 1999: A dipole mode in the tropical Indian Ocean. *Nature*, **401 (6751)**, 360–363, doi:10.1038/43854, URL http://www.nature.com/articles/43854.

Schott, F. A., S.-P. Xie, and J. P. McCreary, 2009: Indian Ocean circulation and climate variability. *Reviews of Geophysics*, **47 (1)**, RG1002, doi:10.1029/2007RG000245, URL http://doi.wiley.com/10.1029/2007RG000245.

Siler, N., Y. Kosaka, S. P. Xie, and X. Li, 2017: Tropical ocean contributions to California's surprisingly dry El Niño of 2015/16. *Journal of Climate*, **30 (24)**, 10 067–10 079, doi:10.1175/JCLI-D-17-0177.1.

Sorensen, C. J., M. J. Borbor-Cordova, E. Calvello-Hynes, A. Diaz, J. Lemery, and A. M. Stewart-Ibarra, 2017: Climate Variability, Vulnerability, and Natural Disasters: A Case Study of Zika Virus in Manabi, Ecuador Following the 2016 Earthquake. *GeoHealth*, **1 (8)**, 298–304, doi:10.1002/2017GH000104, URL http://doi.wiley.com/10.1002/2017GH000104.

Tozier de la Poterie, A. S., W. E. Jjemba, R. Singh, E. Coughlan de Perez, C. V. Costella, and J. Arrighi, 2018: Understanding the use of 2015–2016 El Niño forecasts in shaping early humanitarian action in Eastern and Southern Africa. *International Journal of Disaster Risk Reduction*, **30**, 81–94, doi:10.1016/j.ijdrr.2018.02.025, URL https://www.sciencedirect.com/science/article/pii/S2212420918302140https://linkinghub.elsevier.com/retrieve/pii/S2212420918302140.

Accepted for publication in *Journal of Climate*. DOI 10.1175/JCLI-D-19-0201.1.

589 Tseng, Y.-H., R. Ding, and X.-m. Huang, 2017: The warm Blob in the northeast Pacific–the
590 bridge leading to the 2015/16 El Niño. *Environmental Research Letters*, **12 (5)**, 054 019, doi:10.
591 1088/1748-9326/aa67c3, URL http://stacks.iop.org/1748-9326/12/i=5/a=054019?key=crossref.
592 cb8bfea1c1421ec0a461ac059296cb2e.

593 Vicente-Serrano, S. M., J. I. López-Moreno, L. Gimeno, R. Nieto, E. Morán-Tejeda, J. Lorenzo-
594 Lacruz, S. Beguería, and C. Azorin-Molina, 2011: A multiscalar global evaluation of the impact
595 of ENSO on droughts. *J. Geophys. Res*, **116**, 20 109, doi:10.1029/2011JD016039, URL https:
596 //agupubs.onlinelibrary.wiley.com/doi/pdf/10.1029/2011JD016039.

597 Wanders, N., and Coauthors, 2017: Forecasting the hydroclimatic signature of the 2015/16 el niño
598 event on the western united states. *Journal of Hydrometeorology*, **18 (1)**, 177–186.

599 Weisheimer, A., N. Schaller, C. O'Reilly, D. A. MacLeod, and T. Palmer, 2017: Atmospheric
600 seasonal forecasts of the twentieth century: multi-decadal variability in predictive skill of the
601 winter North Atlantic Oscillation (NAO) and their potential value for extreme event attribution.
602 *Quarterly Journal of the Royal Meteorological Society*, doi:10.1002/qj.2976.

603 Wolff, C., G. H. Haug, A. Timmermann, J. S. S. Damste, A. Brauer, D. M. Sigman, M. A. Cane,
604 and D. Verschuren, 2011: Reduced Interannual Rainfall Variability in East Africa During the
605 Last Ice Age. *Science*, **333 (6043)**, 743–747, doi:10.1126/science.1203724, URL http://www.
606 sciencemag.org/cgi/doi/10.1126/science.1203724.

607 Zaitchik, B. F., 2017: Madden-Julian Oscillation impacts on tropical African precipitation. 88–102
608 pp., doi:10.1016/j.atmosres.2016.10.002.

609 Zhang, T., and Coauthors, 2018: Predictability and prediction of southern california rains during
610 strong el niño events: a focus on the failed 2016 winter rains. *Journal of Climate*, **31 (2)**, 555–

Accepted for publication in *Journal of Climate*. DOI 10.1175/JCLI-D-19-0201.1.

574.

Accepted for publication in *Journal of Climate*. DOI 10.1175/JCLI-D-19-0201.1.

LIST OF FIGURES

Accepted for publication in *Journal of Climate*. DOI 10.1175/JCLI-D-19-0201.1.

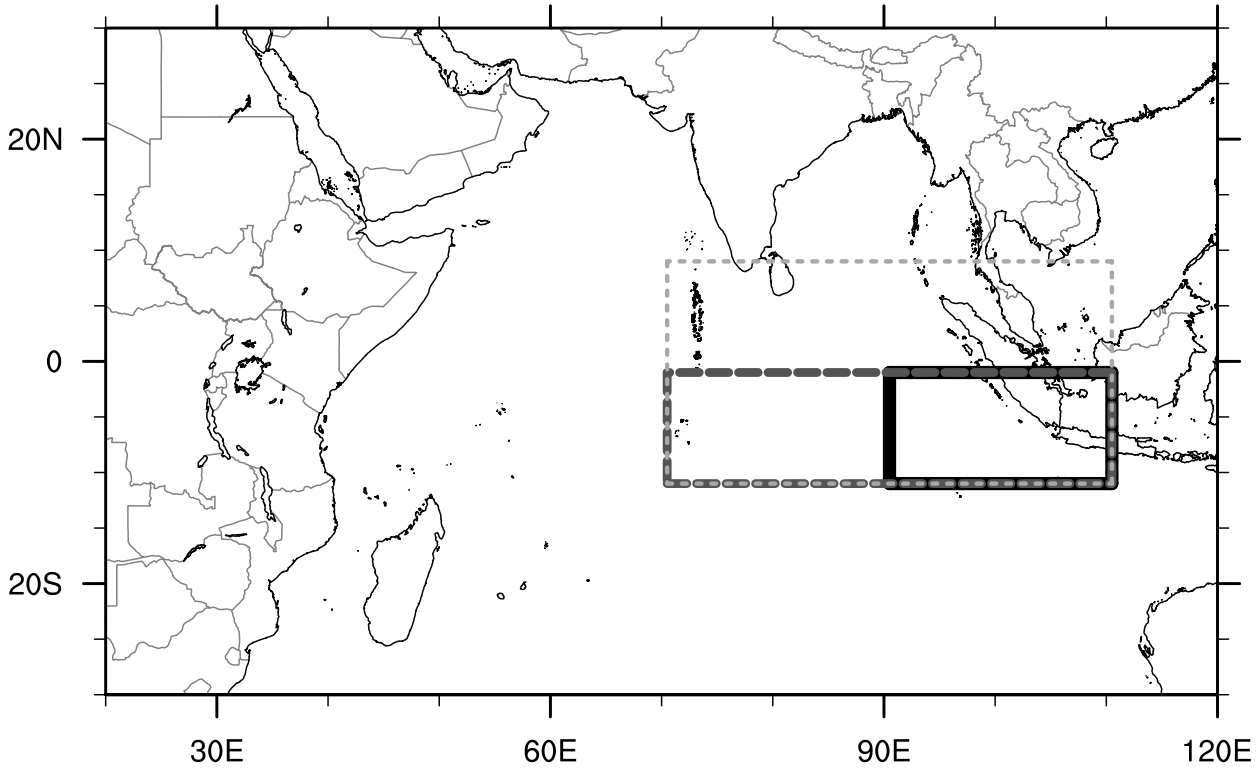

FIG. 1. Regions used for the atmospheric relaxation experiments. The three experiments IOD2, IOD2+ and IOD2++ are shown with the thick black, medium dashed dark grey and thin dashed light grey lines respectively.

Accepted for publication in *Journal of Climate*. DOI 10.1175/JCLI-D-19-0201.1.

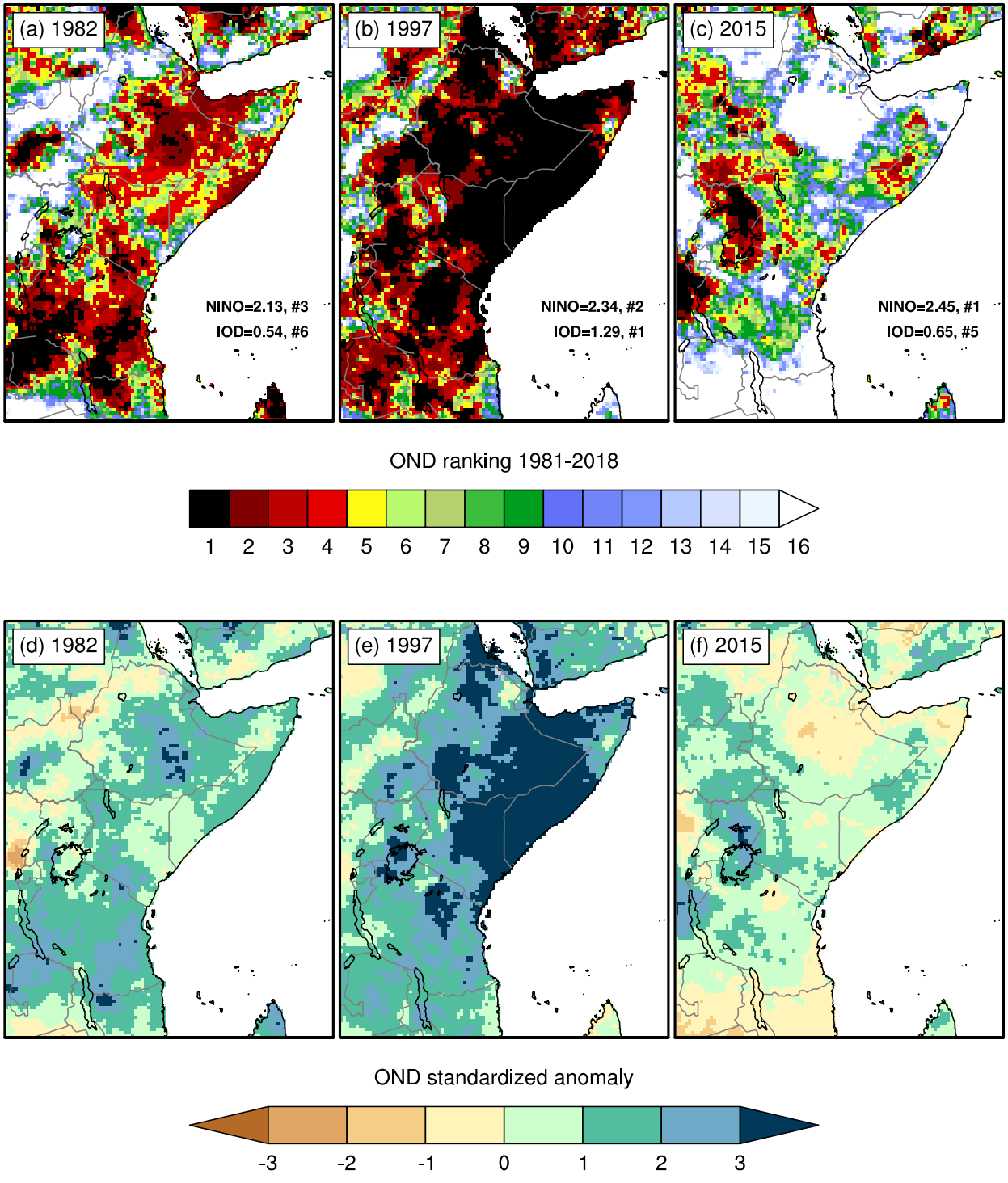

650 FIG. 2. OND rainfall from CHIRPS during three strong El Niño years, (a) 1982 (b) 1997 and (c) 2015,
651 showing the ranking across 1981-2018 (a ranking of 1 indicates the year was the wettest in the record). (d-f)
652 shows the standardized rainfall anomalies for these seasons. Each figure (a-c) also shows the rank and magnitude
653 of the season mean Niño 3.4 and IOD index.

Accepted for publication in *Journal of Climate*. DOI 10.1175/JCLI-D-19-0201.1.

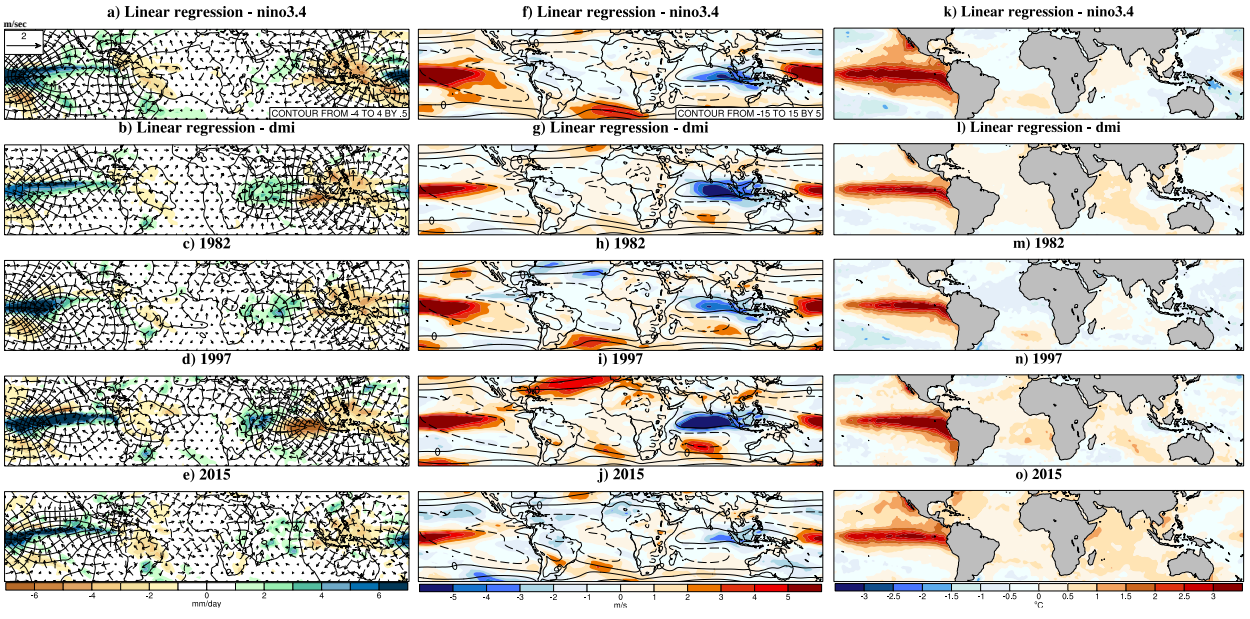

654 FIG. 3. Comparison of different climate variables regressed over 1981-2016 against the Niño 3.4 index (first
655 row) and IOD (second row), with the specific climate anomalies corresponding to 1982 (third row), 1997 (fourth
656 row) and 2015 (fifth row). Left column: rainfall (color, mm/day), divergent component of the wind at 850mb
657 (vectors in m/s). Contours of positive and negative 850mb velocity potential are shown in steps of $0.5 \times 10^6 m^2/s$
658 as solid and dashed lines, with zero indicated by the thicker black contour. Middle Column shows the 850mb
659 zonal wind anomaly and climatological mean with colours and contours respectively; contours indicate an in-
660 terval of 5m/s (solid/dashed showing positive/negative with the thicker line indicating the zero contour). Right
661 column: SST (°C). Note that linear regression coefficients were multiplied by an (arbitrary) factor of 3 to allow
662 visual comparison with the anomalies.

Accepted for publication in *Journal of Climate*. DOI 10.1175/JCLI-D-19-0201.1.

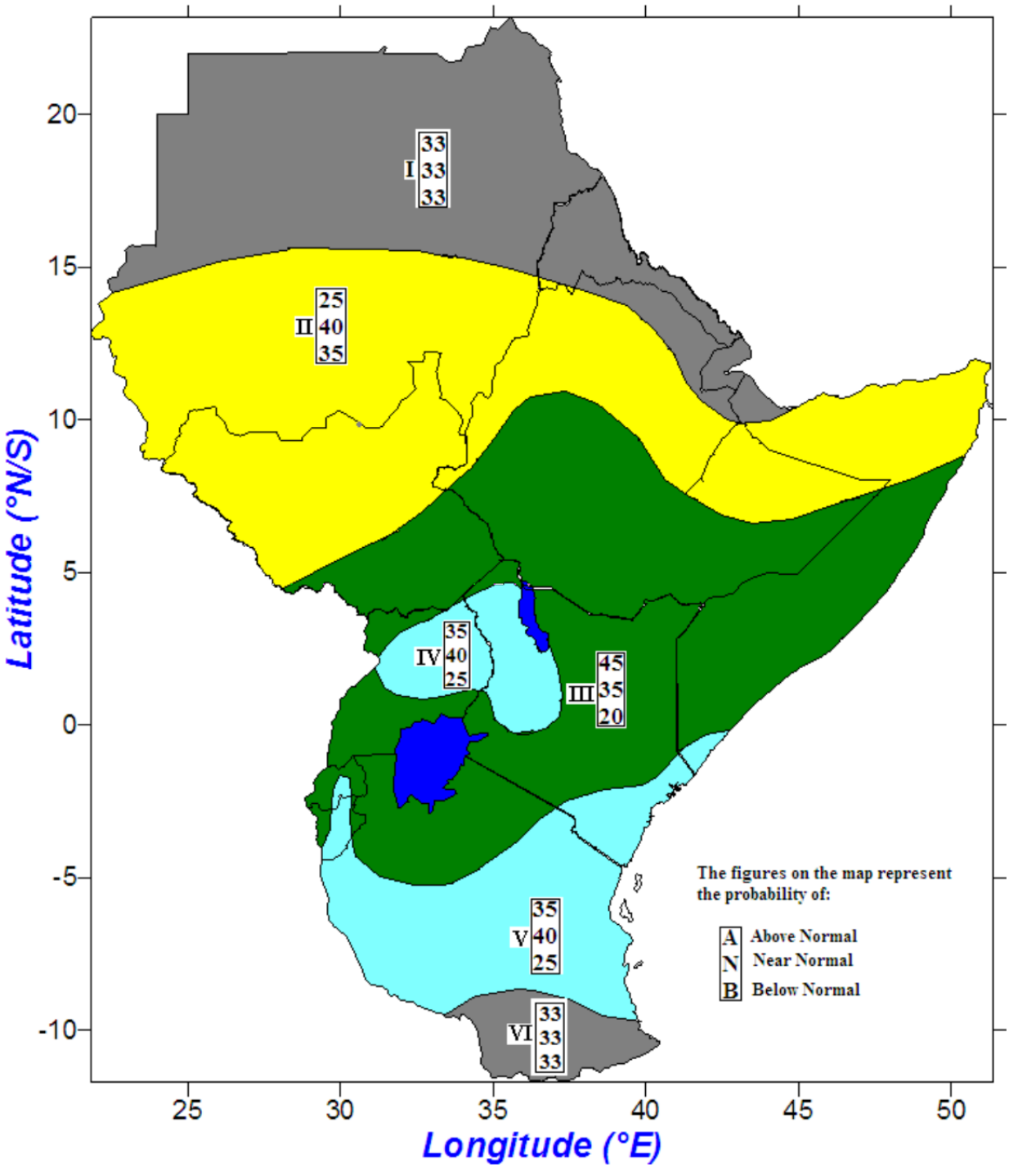

663 FIG. 4. Consensus forecast from GHACOF41, held in preparation for the short rains (OND) 2015 (ICPAC
664 (2015)).

Accepted for publication in *Journal of Climate*. DOI 10.1175/JCLI-D-19-0201.1.

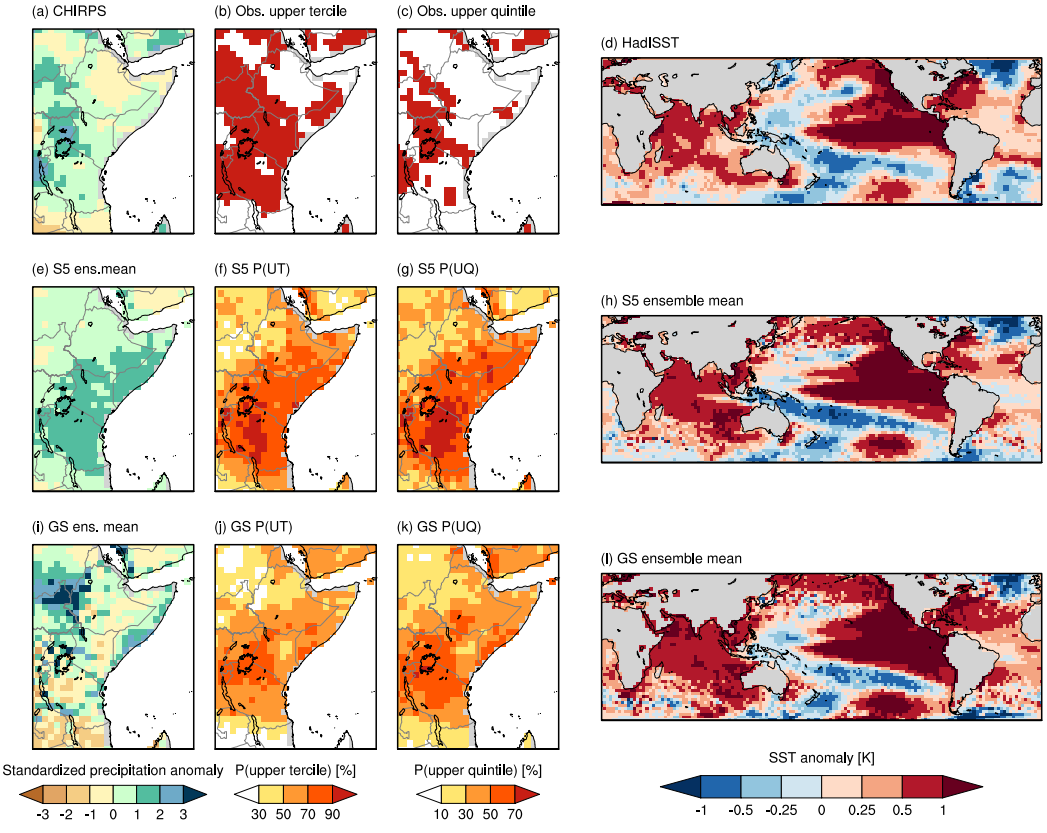

665 FIG. 5. OND 2015 precipitation and SST in observations (a-d), SEAS5 (e-h) and GloSea5 (i-l). The left
666 column shows standardized OND precipitation anomalies in CHIRPS (a) and the ensemble mean from the two
667 systems (e, i). The central two columns shows regions where OND rainfall was in the upper tercile and quintile
668 in CHIRPS (b-c) and the forecast probabilities for those events in the two forecast systems (f-g, i-j; note the
669 different colour scale). The right column shows OND SST anomalies in HadISST (d) and the ensemble mean
670 SST anomaly in SEAS5 and GloSea5 (h, l).

Accepted for publication in *Journal of Climate*. DOI 10.1175/JCLI-D-19-0201.1.

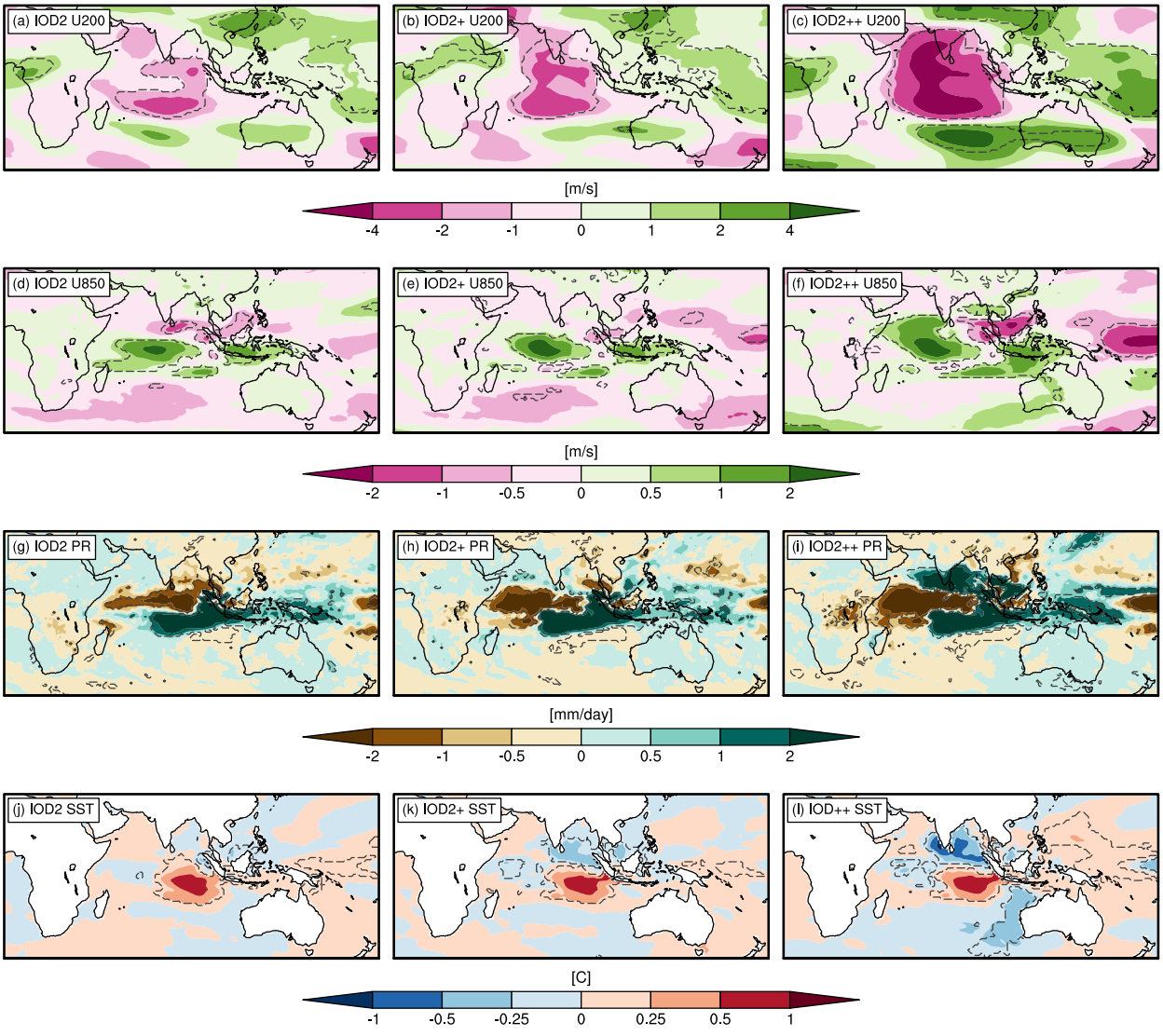

FIG. 6. Results from the relaxation experiments for reforecasts of OND 2015. Differences of the mean of each experiment 25-member ensemble against the mean of the 25-member control ensemble run are shown, for 200mb zonal wind (a-c), 850mb zonal wind (d-f), precipitation (g-i) and SST (j-l). Results for the three experiments IOD2, IOD2+ and IOD2++ are shown in left, central and right columns respectively. In each case differences between the means of the two ensembles which are significant at the 99% level based on a two-sided t-test are indicated by a dashed grey contour line.

Accepted for publication in *Journal of Climate*. DOI 10.1175/JCLI-D-19-0201.1.